# Power Transmitter Design for Underwater WPT

Miguel Silva
*INESC TEC and FEUP*
Porto, Portugal
up201403909@fe.up.pt

Cândido Duarte
*INESC TEC and FEUP*
Porto, Portugal
candidoduarte@fe.up.pt

Francisco Gonçalves
*INESC TEC and FEUP*
Porto, Portugal
frpg@fe.up.pt

Vasco Correia
*INESC TEC and FEUP*
Porto, Portugal
vasco.m.correia@inesctec.pt

Luís Pessoa
*INESC TEC*
Porto, Portugal
lpessoa@inesctec.pt

***Abstract*—The present work addresses the development of a power inverter, specifically designed for underwater wireless power transfer (WPT) by means of magnetic resonant coupling, having salt water as the transmission medium. Series capacitors are used both at the primary and secondary sides of the coupled coils, but with the operating frequency defined above resonance. The design makes use of the impedance of load and resonant coupling coils to establish class-DE conditions in a full-bridge inverter. Experimental WPT results with salt water separating the primary and secondary sides demonstrated dc-to-dc efficiencies in the range of 80 to 86 percent, i.e. taking into account rectification at the secondary side and losses in water, achieving output power levels in the range of 20 to 80 Watt at operating frequencies between 150 and 210 kilohertz.**

***Index Terms*—Class-DE power inverter, underwater WPT.**

## I. Introduction

Underwater wireless power transfer (WPT) in ocean is critically limited by the energy dissipated in salt water. This conductive medium is responsible for most of the power losses, signicantly increasing with the distance between power transmitter and receiver. A careful design of the coil pair with proper geometry and adequate choice of materials can effectively help in reducing these losses, but only up to some degree.

The target scenario addressed in this work consists of a wireless sensor network in which an autonomous underwater vehicle (AUV) travels in the ocean to energize sensors, arbitrarily located at seabed, by means of underwater WPT. This is achieved by virtue of an inductive resonant link, with the energy being transferred from a transmitting coil, at the AUV, to a receiving coil at each sensor node. Aside from the impact of the salt water conductivity, another important obstacle tends to be the lack of satisfactory predictability on the load impedance seen from the transmitter. This is essentially due to coil misalignments and fluctuations of the AUV [1]–[3], which varies the coupling value between coils, in addition to an eventual heterogeneity of sensor energy profiles and time variability of loading demands. As such, the nominal conditions at which the coupling coils are designed cannot be maintained along with the complete WPT process and, therefore, the power efficiency is degraded.

This work is financed by the ERDF – European Regional Development Fund through the Operational Programme for Competitiveness and Internationalisation – COMPETE 2020 Programme and by National Funds through the Portuguese funding agency, FCT – Fundação para a Ciência e a Tecnologia within project POCI-01-0145-FEDER-031971.

Two important limitations of underwater WPT have been identified, i.e. *i)* the energy losses in the water medium, and *ii)* the impedance uncertainty that takes place at transmitter. But a third aspect is equally relevant, which is the power efficiency of dc-ac conversion at the transmitter itself. At the AUV, a power inverter converts dc power from a battery pack into the ac power to be delivered. To be efficient, this conversion process requires the mitigation of two common power dissipation mechanisms: the conduction and switching losses. The former is commonly minimised through the use of MOSFET devices with reduced $R_{\mathrm{DS}}$, whereas the latter can be decreased by choosing a suitable power inverter architecture. This is precisely the main focus of the present work.

In air, as well as in fresh water, higher frequency of operation usually reflects on higher (unloaded) quality factors of the coupling coils. As a consequence, the link efficiency established with the coupling coils is improved by choosing an operating frequency relatively high, in the order of a few MHz. In contrast, when salt water is the WPT medium, above certain frequency the ac losses tend to overcome the quality factor improvement just mentioned. This imposes the use of a reduced frequency of operation in underwater WPT for salt water environments, in the range of tens to a few hundred kHz [4]. Therefore, in these conditions it is appropriate to choose a power inverter relying on voltage-mode class D (VMCD), as it is a straightforward option and it is relatively simple to control at low frequencies [5], [6] comparing to other topologies, for instance in current mode [7]. However, the main hindrance to the power conversion efciency is due to nonzero voltage at the switching instant. Although zero voltage switching (ZVS) conditions can be achieved with operation frequencies slightly above resonance, the optimum point is not easily reached, at least in a systematic way. Strategies relying on the voltage monitoring of the switching node are difcult to employ because of bandwidth restrictions [8], and impractical access to the load at the secondary side also reveals itself as an obstacle to ZVS sensing.

In the present work we focus on the development of an efficient power inverter that takes into account the coupling coils, by incorporating them into the load network design. We propose the use of a class-DE inverter, which uses similar class-E conditions on top of a VMCD power converter, i.e. imposing ZVS and zero-voltage derivative switching (ZVDS) in the design of a power transmitter for the purpose of underwater WPT with salt water between coils.

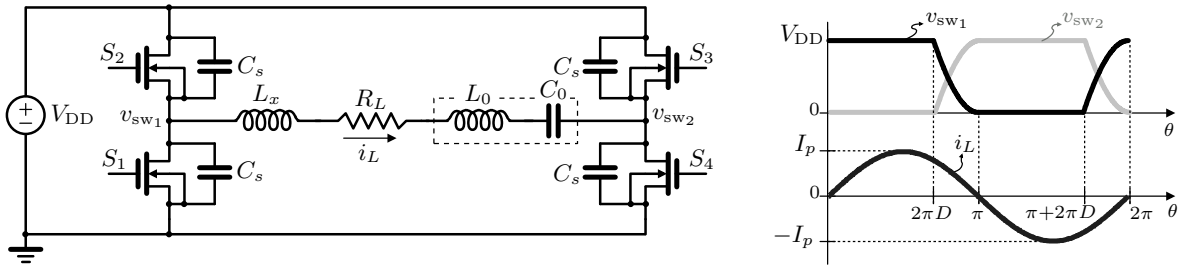


(a) (b)

Fig. 1. Class DE (a) full-bridge circuit and (b) typical time-domain waveforms.

## II. Analysis of the Class-DE Power Inverter

The class-DE amplification was introduced by Zhukov and Kozyrev [9]. Basically, it consists on the VMCD topology with switching operation similar to the class E. The key idea is to allow the shunt capacitances discharge/charge to the next desired voltage level, so that when the switching operation occurs the shunt capacitances are completely discharged. This ZVS condition minimizes the switching losses, which may be dominant whenever the dc voltage is large or the operation frequency is high.

Fig. 1(a) depicts a full-bridge class-DE circuit, and Fig. 1(b) shows the circuit waveforms. An ideal analysis is based upon the assumptions:

1) the MOSFETs ($S_1$ to $S_4$) operate as ideal switches, i.e. with null conduction resistance and instantaneous switching transitions;
2) $S_1$ and $S_3$ form a pair of switches; $S_2$ and $S_4$ form another one. Each transistor from a pair is driven the same way;
3) the shunt capacitance of each MOSFET is considered linear (and all equal to $C_s$)[1];
4) the load network has a sufficiently high quality factor such as one can guarantee a pure sinusoidal current flowing in the load network.

The load network comprises an LC tank formed by $L_0$ and $C_0$, resonant at the switching frequency. An additional inductance $L_x$ is included in the network, to make it inductive at the operating frequency. Satisfying the ZVS criteria, the current at the load network $i_L(\theta)$ is sinusoidal an considered to be null at the off-on transitions, i.e.

$$i_L(\theta) = I_p \sin(\theta) \tag{1}$$

The MOSFETs are driven with similar duty-factors ($D$), with $S_1$ and $S_3$ driven the same way, and $S_2$ and $S_4$ driven with half-period delay. Taking in account that all the charge from the shunt capacitors is shared with the load, the output power at the load is given by

$$P_{\rm out} = \frac{2\omega C_s V_{\rm DD}^2}{\pi} \cdot \left( \frac{\sin(2\pi D)}{1+\cos(2\pi D)} \right)^2 \tag{2}$$

[1]A capacitor can be used in parallel with the device. We will denote $C_s$ here as the total capacitance, i.e. any added capacitance plus the output capacitance of the device itself.

The class-DE load impedance can be obtained as follows

$$\begin{aligned} \mathbf{Z_L} &= R_L + jX_L \\ &= \frac{1}{2\pi\omega C_s} \cdot \Big\{ 2\sin^2(2\pi D) + j\big[2\pi(1-2D) + \sin(4\pi D)\big] \Big\} \end{aligned} \tag{3}$$

The load resistance $R_L$ is directly determined from (3) as follows

$$R_L = \mathbf{Re}\{\mathbf{Z_L}\} = \frac{\sin^2(2\pi D)}{\pi\omega C_s} \tag{4}$$

which is maximum for $D = 0.25$ for a fixed $\omega C_s$. Now from (2) and (4), one can get

$$P_{\rm out} = \frac{2}{\pi^2} \cdot \frac{V_{\rm DD}^2}{R_L} \cdot \left( \frac{\sin^2(2\pi D)}{1+\cos(2\pi D)} \right)^2 \tag{5}$$

Assuming the operating frequency defined by the resonance $\omega^2 = 1/(L_0 C_0)$, the additional reactance $L_x$ can be derived from (3) as follows

$$L_x = \mathbf{Im}\{\mathbf{Z_L}/\omega\} = \frac{L_0 C_0}{2\pi C_s} \cdot \Big[ 2\pi(1-2D) + \sin(4\pi D) \Big] \tag{6}$$

which can be be related with $R_L$, or $Q_L$ as

$$L_x = \alpha(D) \cdot \frac{R_L}{\omega} = \frac{\alpha(D)}{1-\alpha(D)} \cdot \frac{L_0}{Q_L} \tag{7}$$

where $Q_L$ is the loaded quality factor of the RLC series of the output network described by

$$Q_L = \frac{\omega(L_0 + L_x)}{R_L} \tag{8}$$

and $\alpha(D)$ is a duty-cycle dependent function given by

$$\alpha(D) = \frac{2\pi(1-2D) + \sin(4\pi D)}{\sin^2(2\pi D)} \tag{9}$$

## III. WPT Class-DE Design

Let us assume the circuit model shown in Fig. 2(a) as an equivalent circuit for the WPT coupling coils, with the primary and secondary series resonances included ($C_1$ and $C_2$). For simplicity, the inductances $L_{11}$ and $L_{22}$ are considered as equal, i.e. $L_{11} = L_{22} = (1-k)L$, where $k$ is the inductive coupling coefficient. Therefore, the mutual inductance is

$$L_{\text{eq}} = \frac{\big[R_m(L_i - kL) + kL(R_2 + R_L)\big](R_2 + R_L + R_m) - L_i R_m(R_2 + R_L) + \omega^2 L_i kL(L_i - kL)}{\omega^2 L_i^2 + (R_2 + R_L + R_m)^2} + L_i - kL \tag{10}$$

$$R_{\text{eq}} = \frac{\omega^2 L_i\big[R_m(L_i - kL) + kL(R_2 + R_L)\big] + R_m(R_2 + R_L)(R_2 + R_L + R_m) - \omega^2 kL(L_i - kL)(R_2 + R_L + R_m)}{\omega^2 L_i^2 + (R_2 + R_L + R_m)^2} + R_1 \tag{11}$$

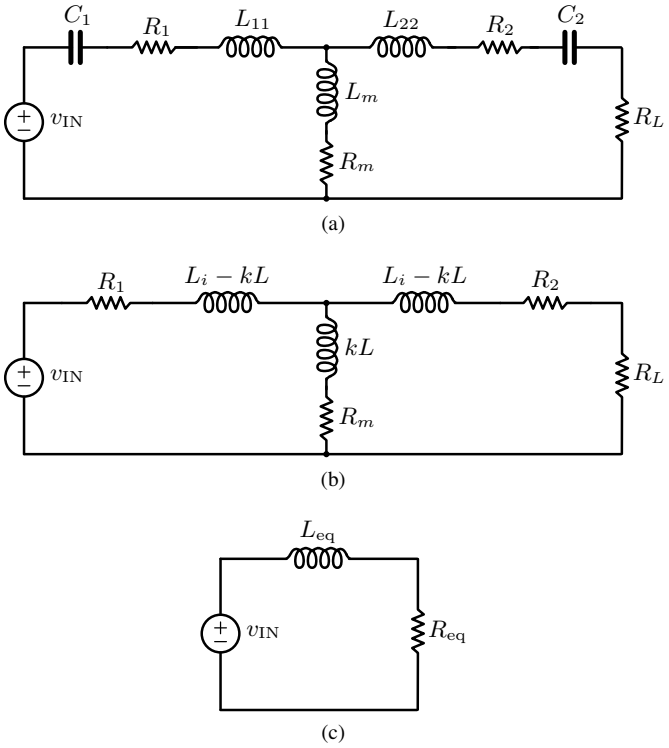


Fig. 2. (a) Coupled coils equivalent model, (b) equivalent circuit valid at frequencies above resonance, and (c) input impedance seen from primary.

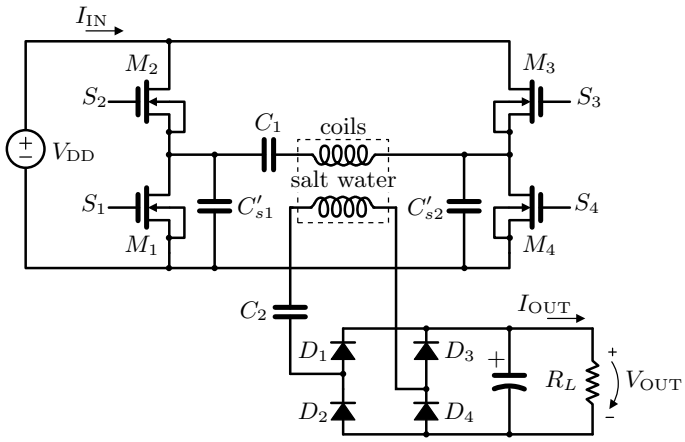


Fig. 3. WPT circuit design for experimental validation.

TABLE I
SYSTEM DEVICES

| device | ref., manufacturer |
|---|---|
| $M_1$, $M_2$, $M_3$, $M_4$ | CSD18536KTT, Texas Instruments |
| $C_1$, $C_2$ | 940C30S68K-F, Cornell Dubilier Electronics |
| $R_L$ | BFA522R, TE Connectivity |
| $D_1$, $D_2$, $D_3$, $D_4$ | FSV10100V On Semiconductor |
| $C'_{s1}$, $C'_{s2}$ | MLCC C412C223K1R5TA7200, Kemet |

simply $L_m = kL$, and $C_1 = C_2 = C$. Let us now impose an operating frequency $\omega$ above resonance $\omega_0$, i.e.

$$\omega > \omega_0 = \frac{1}{\sqrt{LC}} \tag{12}$$

As a result, at the operating frequency the primary and secondary sides will be operated under an inductive regime, which may be represented by the circuit of Fig. 2(b). The equivalent inductance $L_i$ satisfies the following

$$j\omega L_i = j\left(\omega L - \frac{1}{\omega C}\right) \tag{13}$$

Hence, $L_i = L - 1/(\omega^2 C)$. In such circumstances, an equivalent circuit may be determined for the complete coupling system, resulting in a series of an inductor $L_{\text{eq}}$ and a resistor $R_{\text{eq}}$, as shown in Fig. 2(c). Such input inductance and resistance are given in (10) and (11), respectively.

### A. Design Procedure

Comparing the circuits in Fig. 1(a) and Fig. 2(c), it becomes evident that both circuit loads ($R_L$ and $R_{\text{eq}}$) are the same. As such, we can use $R_{\text{eq}}$ of the WPT system to meet the class-DE conditions. $L_{\text{eq}}$ also needs to be equalized for class-DE operation, i.e. it must be equivalent to the earlier derived $L_x$, given in (7). The value chosen for $C_s$ must absorb also the output capacitance of the active devices, although nonlinear.

As a design example, the circuit from Fig. 3 has been implemented. It consists of a full-bridge inverter with multilayer ceramic capacitors (MLCC) added at each leg, $C'_s = 2C_s$. The devices used in this prototype are listed in Table I. The experimental setup is depicted in Fig. 4. A four-layer printed circuit board (PCB) has been produced with the full-bridge inverter. A 32-bit microcontroller (PIC32MZ1024 from Microchip) has been used to generate the pulse-width modulated (PWM) signals, i.e. defining $D$, and monitor current and voltage waveforms. The coupling coils used in this work are shown in Fig. 4, both made of 14-AWG solid copper, with 2 twisted wires using 7 turns, and encapsulated with epoxy. The coupling parameters are summarized in Table II, together with the characterization of the thin-film resonant capacitors. These values were obtained with an electrical characterization with an impedance meter (Keysight E4980AL).

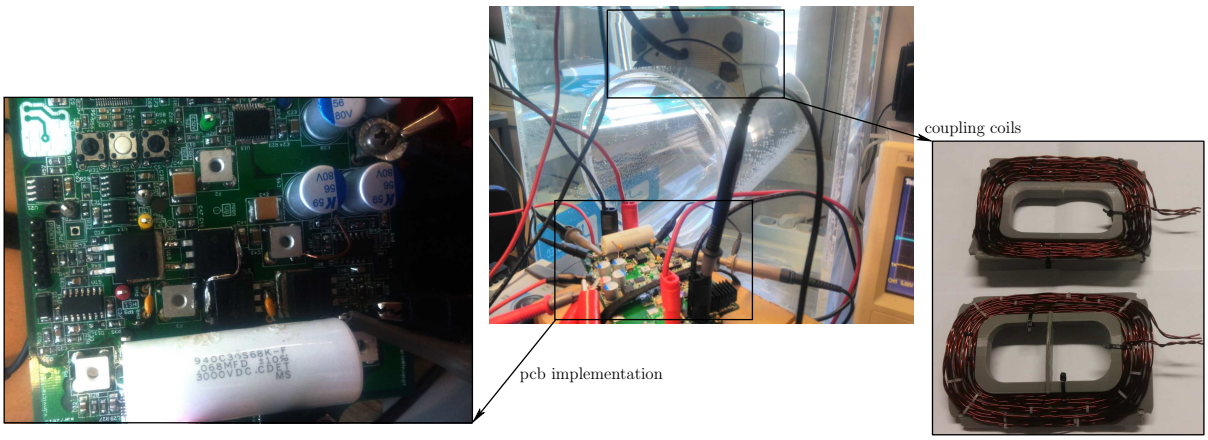


Fig. 4. Experimental setup showing the designed PCB with the power electronics, the coupling coils, encapsulated and before enclosing.

TABLE II
COUPLING PARAMETERS FOR $f = 153\,\text{kHz}$

| | | | | | | |
|---|---|---|---|---|---|---|
| self inductances | $L_1$ | 18.7 | $\mu$H | $L_2$ | 18.7 | $\mu$H |
| parasitic resistances | $R_1$ | 176 | m$\Omega$ | $R_2$ | 165 | m$\Omega$ |
| coil quality factors | $Q_1$ | 102 | | $Q_2$ | 109 | |
| resonant capacitors | $C_1$ | 68.0 | nF | $C_2$ | 68.0 | nF |
| $C_{1,2}$ quality factors | $Q_{C1}$ | 1275 | | $Q_{C2}$ | 1275 | |
| mutual $L$ and $R$ | $L_m$ | 4.42 | $\mu$H | $R_m$ | 83.8 | m$\Omega$ |

TABLE III
RESULTS SUMMARY FOR THE DESIGN EXAMPLE

| | | | | | | | | |
|---|---|---|---|---|---|---|---|---|
| $D$ | 43.0 | % | $f$ | 153 | kHz | $f_0$ | 141 | kHz |
| $V_{DD}$ | 30.0 | V | $I_{IN}$ | 4.82 | A | $P_{IN}$ | 144.5 | W |
| $V_{OUT}$ | 48.2 | W | $I_{OUT}$ | 2.56 | A | $P_{OUT}$ | 123.2 | W |
| $C'_s$=2$C_s$ | 22 | nF | $R_L$ | 18.8 | $\Omega$ | $\eta$ | 85.26 | % |

The coupling coils are perfectly aligned and are surrounded by salt water. The surrounded conductive medium not only degrades the quality factor of each coil [1], it also introduces losses due to resistive coupling. The distance between coils is 4 cm inside the epoxy enclosure, the coils. The cylindrical hollow in Fig. 4 represents the AUV structure, with an external diameter of 20 cm. The results for the design example are summarized in Table III. The reported efficiency takes into account the losses not only in the inverter, but also in the water and in the rectifier. A time-domain waveform for the example is depicted in Fig. 5.

Several tests have been conducted to test the class DE using different parameters. The same inverter tuned as a class D, operating at the resonance frequency $f_0$, is used as a comparison. Fig. 6 depicts the efficiency results for different capacitances $C'_s$, for different $R_L$, $\omega$ and $D$ – lower $C'_s$ tends to higher efficiency, and most of the cases have better efficiency than the class D, due to ZVS (for these results, $V_{DD} = 22\,\text{V}$). Fig. 7 provides the measured results for all the parameters swept.

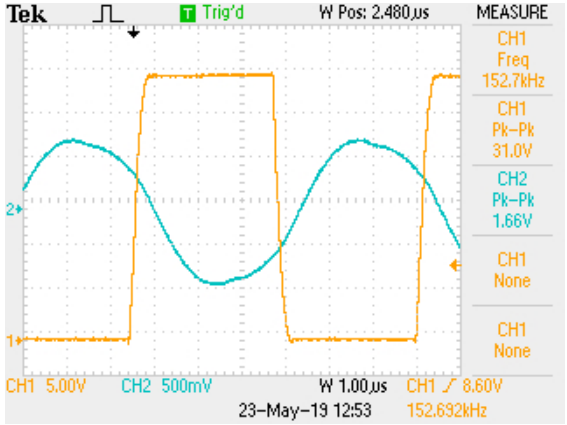


Fig. 5. Measured time-domain waveforms: (a) voltage waveform at a switching node and (b) current at the primary side.

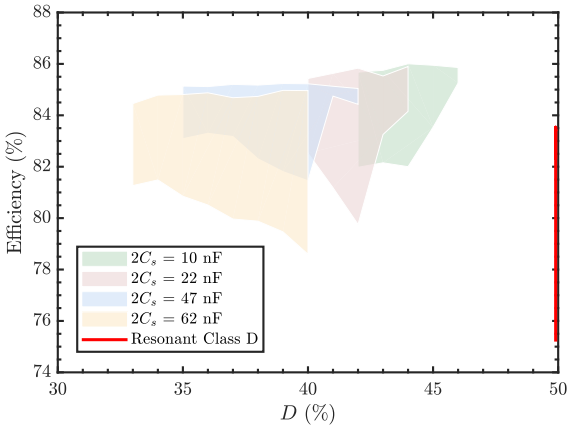


Fig. 6. Efficiency regions for each tested $C_s$ value. Different points for each $D$ were obtained with different frequencies and loads. Class D points were obtained at the resonant frequency with different loads in the same range.

## IV. CONCLUSION

In this work the design of a full-bridge class-DE power inverter is presented for underwater WPT in salt water. In-

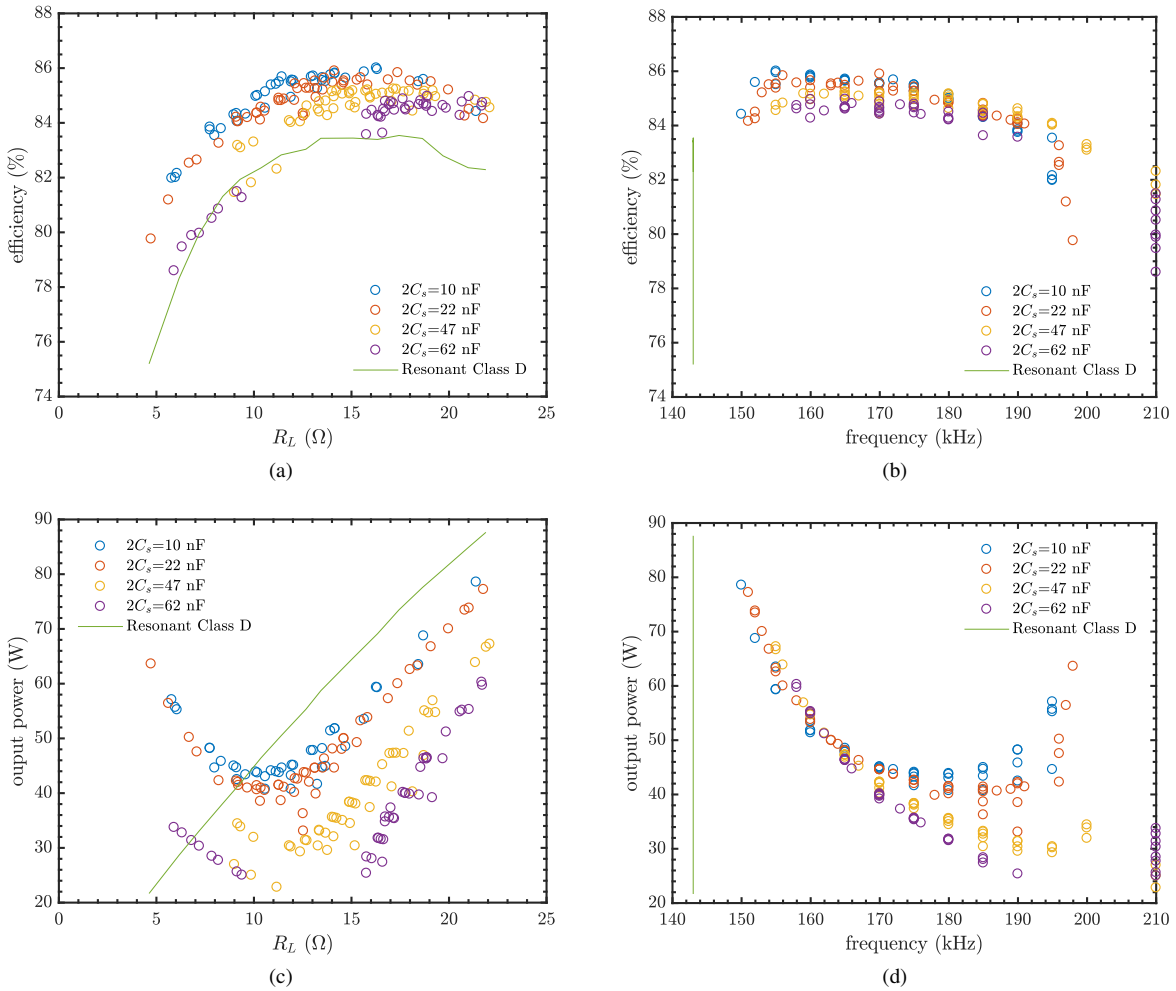


Fig. 7. Class-DE and Class D for different operation parameters.

stead of adding a fixed-value reactance to meet the class-DE conditions, the coupling coils were considered to obtain the required phase shift. The experimental results suggest that both the frequency and duty-cycle can be explored as degrees of freedom to optimize the efficiency of the WPT application.

## Acknowledgment

The authors acknowledge the assistance and resources made available by TEC4SEA in support of this work. This infrastructure is financed by FEDER funds through Programa Operacional Regional do Norte – NORTE 2020 and Programa Operacional Regional do Algarve – ALGARVE21, and by National funds through FCT – Fundação para a Ciência e a Tecnologia (NORTE-01-0145-FEDER-022097).

## References

[1] T. Ressurreição, F. Gonçalves, C. Duarte, R. Gonçalves, R. Gomes, R. Santos, R. Esteves, P. Pinto, I. Oliveira, and L. M. Pessoa, "System design for wireless powering of AUVs," in *OCEANS*, Aberdeen, United Kingdom, Jun 2017, pp. 1–6.

[2] C. Duarte, F. Gonçalves, T. R. ao, R. Gomes, V. Correia, R. Gonçalves, and R. Santos, "A study on load modulation for underwater wireless power transfer," in *OCEANS*, Aberdeen, United Kingdom, Jun 2017, pp. 1–4.

[3] C. Cai, M. Qin, S. Wu, and Z. Yang, "A strong misalignmentt tolerance magnetic coupler for autonomous underwater vehicle wireless power transfer system," in *IEEE International Power Electronics and Application Conference and Exposition (PEAC'2018)*, Nov 2018, pp. 1–5.

[4] F. Gonçalves, A. Pereira, A. Morais, C. Duarte, R. Gomes, and L. M. Pessoa, "An adaptive system for underwater wireless power transfer," in *8th International Congress on Ultra Modern Telecommunications and Control Systems*, Lisbon, Portugal, Oct 2016, pp. 101–105.

[5] A. Pereira, C. Duarte, P. Costa, and W. Gora, "Performance improvement of a buck converter using Kalman filtering," *International Journal of Power Electronics*, vol. 8, no. 2, pp. 87–106, Mar 2017. [Online]. Available: http://www.inderscience.com/info/inarticle.php?artid=82931

[6] G. Sanborn and A. Phipps, "Standards and methods of power control for variable power bidirectional wireless power transfer," in *IEEE Wireless Power Transfer Conference (WPTC'2017)*, May 2017, pp. 1–4.

[7] D. Oliveira, C. Duarte, V. G. Tavares, and P. G. de Oliveira, "Design of a current-mode class-D power amplifier in RF-CMOS," in *Proceedings of the XXIV Conference on Design of Circuits and Integrated Systems (DCIS'2009)*, Zaragoza, Spain, Nov 2009, pp. 418–422.

[8] P. Amaral, C. Duarte, and P. Costa, "On the impact of timer resolution in the efficiency optimization of synchronous buck converters," *International Journal of Power Electronics and Drive Systems*, vol. 6, no. 4, pp. 693–702, Dec 2015.

[9] S. Zhukov and V. Kozyrev, "Push-pull switching generator without switching losses," *Poluprovodnikovye Pribory v. Tekhnike Elektrosvyazi*, vol. 15, pp. 95–107, 1975, in Russian.